

Impact of Symmetry and Donor Set on the Electronic Energy Levels in Nine-coordinated Eu(III) and Sm(III) Crystals Structures Determined from Single Crystal Luminescence Spectra

Sabina Svava Mortensen, Villads R. M. Nielsen, and Thomas Just Sørensen*

Lanthanide luminescence is characterised by “forbidden” $4f-4f$ transitions and a complicated electronic structure. Our understanding of trivalent lanthanide(III) ions luminescence is centered on Eu^{3+} because absorbing and emitting transition in Eu^{3+} occur from a single electronic energy levels. In Sm^{3+} both absorbing and emitting multiplets have a larger multiplicity. A transition from the first emitting state multiplet to the ground state multiplet will result in nine lines for a Sm^{3+} complex. In this study, high resolution emission and excitation spectra were used to determine the electronic energy levels for the ground state multiplet and first excited state multiplet in four Sm^{3+} compounds with varying donor set and site symmetry. This was achieved by the use of Boltzmann distribution population analysis and experimentally determined transition probabilities from emission and excitation spectra. Using this analysis it was possible to show the effect of changing three oxygen atoms with three nitrogen atoms in the tricapping donor set for compounds with the same Trigonal Tricapped Prism (TTP) site symmetry on the crystal field splitting in both Eu^{3+} and Sm^{3+} crystals. This work celebrates the 40 year anniversary for the first report of $[\text{Eu}(\text{ODA})_3]^{3-}$ luminescence by Kirby and Richardson.

Introduction

Lanthanide luminescence fascinates as it is characterised by sharp bands in the luminescence spectra and forbidden transitions with long luminescent lifetimes.²⁻⁹ The similar properties, explained by the similar electron configuration of the lanthanide(III) ions,^{2,3} are exploited in applications including bioassay, bioimaging, and anti-counterfeiting technologies.^{5, 6, 10-16} The applications rely on our ability to understand of the complicated molecular and electronic structure of the lanthanide(III) ions.^{4, 13, 17-22} While the electronic splitting caused by the strong spin-orbit coupling observed as bands in the luminescence spectra has been extensively studied for the lanthanide(III) ions,^{5, 6, 23, 24} the spectral fine structure from the crystal field splitting of the electronic energy levels of the spin-orbit defined 5L_J multiplet into the individual electronic states, defined by m_J , still remains a puzzle.^{8, 9, 25}

The site symmetry, the coordination geometry, and the donor atoms of a lanthanide(III) complexes—their molecular structure—determines the crystal field splitting.²⁶ If the symmetry is low, more lines will be resolved in the luminescence spectra, while higher symmetry creates degenerate states and fewer bands.²⁷⁻³⁰ The knowledge of trivalent lanthanide(III) ions photophysics is still centred around the Eu^{3+} ion.^{13, 24, 27, 31-33} For Eu^{3+} the transition from the ground state (7F_0) to the first emitting state (5D_0) can be observed as a single line, as both states are non-degenerate.^{34, 35} This makes the interpretation of Eu^{3+} ion luminescence spectra simpler than for other lanthanide(III) ions.^{27, 36} The non-degenerate ground and emitting state combined with the fact that the Eu^{3+} ion has been comprehensively studied, makes it a good starting

point for broadening the understanding of other trivalent lanthanide(III) ions.^{13, 24, 27, 31-33}

In contrast to Eu^{3+} , Sm^{3+} has $^6H_{5/2}$ as absorbing state multiplet and $^4G_{5/2}$ as the emitting state multiplet.^{5, 28-30, 36-38} Both multiplets contains tree Kramers levels. For Eu^{3+} the site symmetry can be evaluated directly from the number of observed lines in a given band, as this depends on the site symmetry.^{24, 27, 31, 39, 40} In general, for Sm^{3+} the maximum splitting of a multiplet in the absence of a magnetic field is expected, calculated as $(2J+1)/2$ for the Kramers ions/half integer J lanthanide ions.^{9, 37} This eliminates the possibility of understanding the effect of site symmetry only from the number of lines present in a multiplet. A transition from the emitting multiplet to the lowest energy multiplet: $^4G_{5/2} \rightarrow ^6H_{5/2}$, will result in nine lines for a Sm^{3+} complex.⁴¹ Determining the spectral fine structure for the electronic transitions can be difficult and Sm^{3+} luminescence remains less explored.^{37, 41-45} The other bands in the Sm^{3+} luminescence emission spectrum has maximum splitting of twelve, fifteen, and eighteen for $^6H_{7/2}$, $^6H_{9/2}$, and $^6H_{11/2}$ respectively. As the multiplets of Sm^{3+} contain more than one level, there will be a difference in the population between these states. The population of a certain state is given by the Boltzmann distribution, which depends on the energy between the states and the temperature. The spectra can be simplified using cryogenic temperatures e.g. at 77 K only some of the three $\pm m_J$ levels in $^4G_{5/2}$ and $^6H_{5/2}$ will be populated and thus transitions from higher electronic energy levels may not have an observable intensity in the spectra. The intensity of any line depends on both transition probability and population. In the ideal case, the spectra originates from a single state and only the energy levels in the final multiplet is observed.^{9, 37, 46-49}

Further, analysis relying on the Boltzmann distribution can be used to resolve the electronic structure if both emission and excitation spectra are available.⁴⁹

To investigate the electronic structure of Sm^{3+} , four compounds with different symmetry and the donor sets, but with the same coordination geometry were prepared and crystallised, see Figure 1. To be able to contrast and compare, we also prepared corresponding Eu^{3+} compounds. By using what is known for Eu^{3+} as a symmetry probe,^{24, 27, 31, 39, 40} the Eu^{3+} model system allow us to expand the knowledge about Sm^{3+} .

The series is composed of two compounds with a Trigonal Tricapped Prismatic **TTP** coordination geometry, $\text{Na}_3[\text{Ln}(\text{ODA})_3]\cdot 7\text{H}_2\text{O}$ and $\text{Cs}_3[\text{Ln}(\text{DPA})_3]\cdot 9\text{H}_2\text{O}$, but with different donor sets and symmetries. The $\text{Na}_3[\text{Ln}(\text{ODA})_3]\cdot 7\text{H}_2\text{O}$ compound has a donor set consisting of nine oxygen atoms. The $\text{Cs}_3[\text{Ln}(\text{DPA})_3]\cdot 9\text{H}_2\text{O}$ compound a donor set with three nitrogen atoms in the capping layer and six oxygen atoms in the two trigonal layers.^{17, 18, 50, 51} The other half of the series is two compounds with capped square-antiprismatic **cSAP** geometry with different donor sets: $\text{Na}[\text{Ln}(\text{DOTA})\text{H}_2\text{O}]\cdot 4\text{H}_2\text{O}$ and $\text{Na}[\text{Ln}(\text{EDTA})(\text{H}_2\text{O})_3]\cdot 5\text{H}_2\text{O}$. The $\text{Na}[\text{Ln}(\text{DOTA})\text{H}_2\text{O}]\cdot 4\text{H}_2\text{O}$ compound has a donor set consisting of four nitrogen atoms, four oxygen atoms, and a capping oxygen, and $\text{Na}[\text{Ln}(\text{EDTA})(\text{H}_2\text{O})_3]\cdot 5\text{H}_2\text{O}$ compound has a mixed oxygen/nitrogen donor set without any apparent symmetry. The single crystal structures were determined, and luminescence spectra were recorded from single crystals and microcrystalline powders. To quantify the symmetry of each compound, both geometry and symmetry deviation values were computed and used to determine the deviation from the ideal TTP and cSAP geometry and the corresponding D_{3h} and C_{4v} point group symmetries.⁵² While the compounds have high symmetry and geometries closed to the idealised coordination polyhedra, none of the four compounds were found to have the previously reported empirically determined crystal field splitting.³⁶

Experimental Section

Synthesis

All chemicals were used as received without further purification.

0.2 M $\text{Eu}(\text{CF}_3\text{SO}_3)_3$ Stock Solution

$\text{Eu}(\text{CF}_3\text{SO}_3)_3$ (2.40 g, 4.00 mmol) (98% from STREM Chemicals) was used to create a 0.20 M stock solution by dissolving the salt in water creating a solution with a volume of 20.0 ± 0.04 ml.

$\text{Na}_3[\text{Eu}(\text{ODA})_3]\cdot 8\text{H}_2\text{O}$ Crystallisation

H_2ODA (0.538 g, 4.01 mmol) (H_2ODA 98% from Sigma Aldrich), $\text{H}_2\text{ODA} = 2,2'$ -oxydiacetic acid/diglycolic acid was used to create a 0.20 M stock solution by dissolving the acid in water to create a solution with a with a volume of 20 ± 0.04 ml with $\text{pH} = 5$ using NaOH (1.0 M). $\text{Na}_3[\text{Eu}(\text{ODA})_3]\cdot 9\text{H}_2\text{O}$ was created by adding 0.5 ml of the 0.20 M $\text{Eu}(\text{CF}_3\text{SO}_3)_3$ to a sample vial with 1.5 ml of the 0.20 M H_2ODA stock. The sample was heated at 80°C for 1 h. The sample vial was placed in container with acetone, placing a lit and left for an acetone diffusion. After 3 day crystals had formed ($N = 3$).

$\text{Cs}_3[\text{Eu}(\text{DPA})_3]\cdot 9\text{H}_2\text{O}$ Crystallisation

H_2DPA (0.669 g, 4.01 mmol) (H_2DPA from Riedel-De Haën Seelze-Hannover), $\text{H}_2\text{DPA} = \text{pyridine-2,6-dicarboxylate}$ was used to create a 0.20 M stock solution by dissolving the acid in water to create a solution with a with a volume of 20 ± 0.04 ml with $\text{pH} = 7$ using NaOH (1.0 M).

Cs_2CO_3 (0.326 g, 1.00 mmol) (Cs_2CO_3 99% from Sigma Aldrich) was used to create a 0.10 M stock solution by dissolving the salt in water to create a solution with a with a volume of 10 ± 0.06 ml.

$\text{Cs}_3[\text{Eu}(\text{DPA})_3]\cdot 9\text{H}_2\text{O}$ was created by adding 0.5 ml of the 0.20 M $\text{Eu}(\text{CF}_3\text{SO}_3)_3$ stock to a sample vial with 1.5 ml of the 0.20 M H_2DPA stock and 2.0 ml of the 0.20 M Cs_2CO_3 stock. The sample was filtered through a Q-Max RR syringe filter from Frisinette and transferred to a sample vial. The sample was heated at 80°C for 1 h. The sample vial was placed in container with acetone,

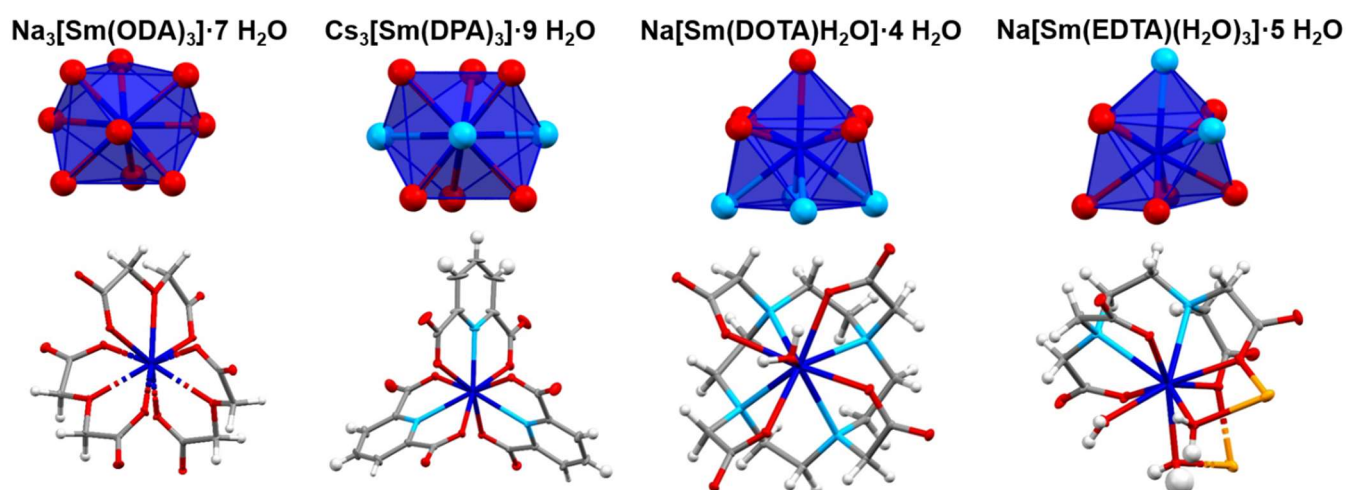


Figure 1. Polyhedra depicting coordination around the Sm^{3+} ion and molecular structure of the compounds: $\text{Na}_3[\text{Sm}(\text{ODA})_3]\cdot 7\text{H}_2\text{O}$, $\text{Cs}_3[\text{Sm}(\text{DPA})_3]\cdot 9\text{H}_2\text{O}$, $\text{Na}[\text{Sm}(\text{DOTA})\text{H}_2\text{O}]\cdot 4\text{H}_2\text{O}$, and $\text{Na}[\text{Sm}(\text{EDTA})(\text{H}_2\text{O})_3]\cdot 5\text{H}_2\text{O}$.

placing a lit and left for an acetone diffusion. After 3 day crystals had formed ($N = 3$).

Na[Eu(DOTA)H₂O]·4H₂O Crystallisation

H₄DOTA (0.80918 g, 2.001·mmol), (H₄DOTA from CheMatech) H₄DOTA = 1,4,7,10-tetraazacyclododecane-N,N',N'',N'''-tetraacetate was used to create a 0.10 M stock solution by dissolving the acid in water to create a solution with a with a volume of 20 ± 0.04 ml with pH = 8 using NaOH (1.0 M). Na[Eu(DOTA)H₂O]·9H₂O was created by adding 1.0 ml of the 0.20 M Eu(CF₃SO₃)₃ stock to a sample vial with 2.0 ml of the 0.1 M H₄DOTA stock. The sample was heated at 80°C for 1 h. The sample vial was placed in container with acetone, placing a lit and left for an acetone diffusion. After 1 day crystals had formed ($N = 3$).

Na[Eu(EDTA)(H₂O)₃]·5H₂O Crystallisation

H₄EDTA (0.26888 g, 0.8045 mmol) (H₄EDTA 98% from STEM Chemicals), H₄EDTA = (2,2',2'',2'''-(ethane-1,2-diylidinitrilo))tetraacetic acid was used to create a 0.20 M stock solution by dissolving the acid in water to create a solution with a with a volume of 20 ± 0.04 ml with pH = 8 using NaOH (1.0 M). Na[Eu(EDTA)(H₂O)₃]·5H₂O was created by adding 1.0 ml of the 0.2 M Eu(CF₃SO₃)₃ stock to a sample vial with 1.0 ml of the 0.20 M H₄EDTA stock. The sample was heated at 80°C for 1 h. The sample vial was placed in container with acetone, placing a lit and left for an acetone diffusion. After 1 day crystals had formed ($N = 3$).

0.2 M Sm(CF₃SO₃)₃ Stock Solution

Sm(CF₃SO₃)₃ (2.39 g, 4.00 mmol) (98% from ABCR) was used to create a 0.20 M stock solution by dissolving the salt in water creating a solution with a volume of 20.0 ± 0.04 ml.

Na₃[Sm(ODA)₃]·7H₂O Crystallisation

H₂ODA (0.538 g, 4.01 mmol) (H₂ODA 98% from Sigma Aldrich), H₂DPA = 2,2'-dioxycetic acid was used to create a 0.20 M stock solution by dissolving the acid in water to create a solution with a with a volume of 20 ± 0.04 ml with pH = 5 using NaOH (1.0 M). Na₃[Sm(ODA)₃]·7H₂O was created by adding 0.5 ml of the 0.20 M Sm(CF₃SO₃)₃ to a sample vial with 1.5 ml of the 0.20 M H₂ODA stock. The sample was heated at 80°C for 1 h. The sample vial was placed in container with acetone, placing a lit and left for an acetone diffusion. After 3 day crystals had formed ($N = 3$).

Cs₃[Sm(DPA)₃]·9H₂O Crystallisation

H₂DPA (0.669 g, 4.01 mmol) (H₂DPA from Riedel-De Haën Seelze-Hannover), H₂DPA = pyridine-2,6-dicarboxylate was used to create a 0.20 M stock solution by dissolving the acid in water to create a solution with a with a volume of 20 ± 0.04 ml with pH = 7 using NaOH (1.0 M).

Cs₂CO₃ (0.326 g, 1.00 mmol) (Cs₂CO₃ 99% from Sigma Aldrich) was used to create a 0.10 M stock solution by dissolving the salt in water to create a solution with a with a volume of 10 ± 0.06 ml.

Cs₃[Sm(DPA)₃]·9H₂O was created by adding 0.5 ml of the 0.20 M Sm(CF₃SO₃)₃ stock to a sample vial with 1.5 ml of the 0.20 M H₂DPA stock and 2.0 ml of the 0.20 M Cs₂CO₃ stock. The sample was filtered through a Q-Max RR syringe filter from Frisnette and transferred to a sample vial. The sample was heated at 80°C

for 1 h. The sample vial was placed in container with acetone, placing a lit and left for an acetone diffusion. After 3 day crystals had formed ($N = 3$).

Na[Sm(DOTA)H₂O]·4H₂O Crystallisation

H₄DOTA (0.80918 g, 2.001·mmol), (H₄DOTA from CheMatech) H₄DOTA = 1,4,7,10-tetraazacyclododecane-N,N',N'',N'''-tetraacetate was used to create a 0.10 M stock solution by dissolving the acid in water to create a solution with a with a volume of 20 ± 0.04 ml with pH = 8 using NaOH (1.0 M). Na[Sm(DOTA)H₂O]·4H₂O was created by adding 1.0 ml of the 0.20 M Sm(CF₃SO₃)₃ stock to a sample vial with 2.0 ml of the 0.1 M H₄DOTA stock. The sample was heated at 80°C for 1 h. The sample vial was placed in container with acetone, placing a lit and left for an acetone diffusion. After 1 day crystals had formed ($N = 3$).

Na[Sm(EDTA)(H₂O)₃]·5H₂O Crystallisation

H₄EDTA (0.26888 g, 0.8045 mmol) (H₄EDTA 98% from STEM Chemicals), H₄EDTA = (2,2',2'',2'''-(ethane-1,2-diylidinitrilo))tetraacetic acid was used to create a 0.20 M stock solution by dissolving the acid in water to create a solution with a with a volume of 20 ± 0.04 ml with pH = 8 using NaOH (1.0 M). Na[Sm(EDTA)(H₂O)₃]·5H₂O was created by adding 1.0 ml of the 0.2 M Sm(CF₃SO₃)₃ stock to a sample vial with 1.0 ml of the 0.20 M H₄EDTA stock. The sample was heated at 80°C for 1 h. The sample vial was placed in container with acetone, placing a lit and left for an acetone diffusion. After 1 day crystals had formed ($N = 3$).

Single Crystal X-ray Diffraction

Single-crystal X-ray diffraction data was collected using a Bruker D8 Venture diffractometer with a PHOTON 100 CMOS detector, a Mo K α high brilliance μ S X-ray tube ($\lambda = 0.71073$ Å), a multilayer X-ray mirror, and the temperature kept at 100 K using an Oxford Cryo system.

The structure was solved using Olex2⁵³ with the ShelXT program⁵⁴ using intrinsic phasing. Refinement was done using the ShelXL refinement package with least square minimisation. Aromatic hydrogens were added automatically using a riding model all other hydrogens were added manually to residual peaks. All other atoms were refined anisotropically.

Symmetry Deviation Analysis

Symmetry deviation values were calculated using AlingIt⁵⁵ after manual rotational optimisation in Mercury.⁵⁶ The geometry in lanthanide(III) complexes were compared to ideal model polyhedral and the values were scaled with the average bond length in the coordinating lanthanide(III) polyhedral. The coordination number (in this case $N = 9$ for all lanthanide(III) complexes) were used to normalise the results. AlingIt implements Eq. 1, after manual rotational optimisation in Mercury, to calculate a symmetry deviation value, σ_{ideal} .⁵⁵

$$\sigma_{ideal}(P - Q) = \sum_{k=1}^N \frac{|Q_k - P_k|^2}{|Q_k - Q_0|^2} \cdot \frac{100}{N} \quad \text{Eq. 1}$$

where P is a point in the ideal structure, and Q is a point in the distorted structure. Q_0 is the origin in the distorted model. For two identical structures, the symmetry deviation value will be zero, $\sigma_{ideal} = 0$.⁵⁵

Point Group Symmetry Analysis

In addition to the geometrical deviation analysis, the fit and structural deviations to symmetry point groups were evaluated.¹ The deviation from symmetry is evaluated with equation 2.

$$\sigma_{sym}(G, Q) = \sum_{s=1}^N \frac{\sigma_{ideal}(Q, \hat{O}_s Q)}{N} \quad \text{Eq. 2}$$

where $\sigma_{ideal}(Q, \hat{O}_s Q)$ is the geometry deviation defined in Eq. 2 between the coordinate set of structure Q and the same set of coordinates that has been operated with the specific symmetry operation \hat{O}_s . The sum is over all N symmetry operations in a point group, G .

Crystal Powders

For both PXRD and Optical spectroscopy the crystals that precipitated in each sample, were collected by vacuum filtration. The crystals were removed from the filter and crushed to a powder.

Powder X-ray Diffraction

The samples for PXRD were filtered crystals crushed to a powder. Data was collected using a Bruker D8 Advance diffractometer using a Cu K α source ($\lambda = 1.5406 \text{ \AA}$) at 293 K with an integration time of 1 s and a resolution of 1500. Samples were measured using a low background silica sample holder.

Spectroscopy for Crystals Crushed to a Powder

After recording PXRD diffractograms, the crystal powders were added to a 5.0 mm diameter NMR quartz tube from Bruker loaded with 2-methyltetrahydrofuran. The resulting suspensions were cooled using liquid nitrogen and measured in a quartz dewar.

Solid-State Single Crystal Spectroscopy

Solid-state single crystal spectroscopy was measured for Eu³⁺ complexes at 293 K. The spectroscopy settings described before were used to measure emission and excitation, respectively. A single crystal was mounted on a crystal mounting loop. The crystal mounting loop was then placed inside the spectrometer. The setup is the same as in our Eu(DPA) paper.⁵⁷

Optical Spectroscopy for Eu³⁺ Samples

Emission and excitation spectra were measured with a xenon arc lamp as the excitation source on a PTI QuantaMaster8075 from Horiba Scientific. For emission spectroscopy an excitation wavelength at 394 nm (25400 cm⁻¹) was used. Emission was detected from 575 nm (17400 cm⁻¹) to 765 nm (14000 cm⁻¹). The emission slits were kept at 1.0 nm for the two outermost slits and 5.0 nm for the middle slit for all samples. The excitation slits were all kept at 4.0 nm for the powder in a glass setup, and 8.0 nm when using single crystals. The voltage bias was kept at

3.200 V for the reference detector. The integration time was kept at 1 s with a step size of 0.1 nm. For excitation spectroscopy an emission wavelength at 614 nm (16900 cm⁻¹) was used. Excitation was detected from 310 nm (32300 cm⁻¹) to 585 nm (17100 cm⁻¹). Emission slits were all kept at 3.0 nm and excitation slits were kept at 1.0 nm for the two outermost slits and 5.0 nm for the middle slit. These settings were used for both the powder in a glass setup and single crystals. The voltage bias was kept at 6.800 V for the reference detector. The integration time was kept at 1 s with a step size of 0.1 nm.

Optical Spectroscopy for Sm³⁺ Samples

For all samples used for optical spectroscopy and luminescence lifetimes, crystals were crushed to a powder and added to a 5.0 mm diameter NMR quartz cylinders from Bruker with 2-methyl tetrahydrofuran glass.

Emission and Excitation on a PTI QuantaMaster8075 from Horiba Scientific

Emission and excitation spectra were measured with a xenon arc lamp as the excitation source on a PTI QuantaMaster8075 from Horiba Scientific. For this set-up spectra were recorded at 77 K using liquid nitrogen to cool the samples and measured using a quartz dewar. For emission spectroscopy an excitation wavelength at 401 nm (24900 cm⁻¹) was used. Emission was detected from 550 nm (18200 cm⁻¹) to 760 nm (13200 cm⁻¹). The emission slits were kept at 1.0 nm for the two outermost slits and 5.0 nm for the middle slit for all samples. The excitation slits were all kept at 8.0 nm. The voltage bias was kept at 3.200 V for the reference detector. The integration time was kept at 1 s with a step size of 0.1 nm. For excitation spectroscopy an emission wavelength at 598 nm (16700 cm⁻¹) was used. Excitation was detected from 250 nm (40000 cm⁻¹) to 590 nm (16900 cm⁻¹). Emission slits were all kept at 8.0 nm and excitation slits were kept at 1.0 nm for the two outermost slits and 5.0 nm for the middle slit. The voltage bias was kept at 6.800 V for the reference detector. The integration time was kept at 1 s with a step size of 0.1 nm. Emission and excitation spectra measured using this set-up can be found in supporting information.

Emission and Excitation on a Custom Build Spectrometer with a Supercontinuum Laser

Emission and excitation spectra was measured using a custom build spectrometer,⁵⁸ equipped with a supercontinuum laser (NKT SuperK Fianium FIU-15) coupled to a tunable band pass filter (NKT LLTF Contrast VIS/SWIR HP8). Samples were measured both at 298 K and cooled to 77 K using liquid nitrogen to cool the samples and measured in a quartz dewar. For emission spectroscopy an excitation wavelength at 463 nm (21600 cm⁻¹) was used with 90% laser power and a maximum repetition rate (78MHz). A 500 nm (20000 cm⁻¹) long pass filter was used. The centre wavelength was set to 640 nm (15600 cm⁻¹). The integration time was kept at 1 s, with 10 exposures per frame and a 0.54 nm resolution. The slit was kept at 5 μm . The intensity was calibrated using the procedure described in ref ⁵⁸. Excitation spectra were measured by scanning the excitation source at 100% laser power from 520 nm (19200 cm⁻¹) to 580 nm (17200 cm⁻¹) through a Python code that connects to the

tunable band pass filter (NKT LLTF Contrast VIS/SWIR HP8) with a 880 nm (11400 cm⁻¹) centre wavelength. A 750 nm (13300 cm⁻¹) long pass filter was used.

The exposure time per data point was 2 s with 1 exposure per frame, and the step size was set to 0.25 nm. The slit was kept at 15 μm. The set-up is described in more detail in ref.^{49, 58}

Luminescence Lifetimes for Eu³⁺ Samples

The luminescence lifetimes were determined using a PTI QuantaMaster8075 from Horiba Scientific. The excitation wavelength was 394 nm (25400 cm⁻¹), and the emission wavelength 598 nm (17100 cm⁻¹). The slits were all kept at 5 nm for both emission and excitation. The time window was from 200 μs to 3000 μs with an integration time of 28 μs. The luminescence lifetimes were fitted using a mono-exponential decay function using the software Origin Lab Pro's ExpDec1 function.⁵⁹ These settings were used for both the powder in a glass setup and single crystals.

Luminescence Lifetimes for Sm³⁺ Samples

The luminescence lifetimes were determined using a TCSPC FluoTime300 from PicoQuant. The excitation wavelength was 405 nm (24700 cm⁻¹), and the emission wavelength 600 nm (16700 cm⁻¹). The luminescence lifetimes were fitted using a mono-exponential decay function using the PicoQuant EasyTau 2 software.⁶⁰

Deconvoluting the Electronic Energy Levels in the Sm³⁺ Compounds using Boltzmann population analysis

To determine which transitions originated from which electronic energy levels (m_j) in the ground state multiplet (⁶H_{5/2}) and the first emitting state multiplet (⁴G_{5/2}), we used our Boltzmann analysis procedure.⁴⁹ Briefly summarised: The calculated population from the Boltzmann distribution was compared to the observed difference in emission and excitation intensity. The observed relative transition intensities for emission and excitation were extracted from the Voigt functions. The relative emission intensity for a transition from j to i is assumed to be proportional to the population of the state, j , at a given temperature and the relative emission transition probability. The same is assumed for the excitation intensity. $A_{i \rightarrow j}$ is the absorption transition probability for a from j to i , and $B_{i \leftarrow j}$ is the emission transition probability for a from i to j . It is assumed that the ratio of transition probability between two levels i and j is the same for emission and excitation. For Sm³⁺ specifically, the observed thermal population for the ground state multiplet, ⁶H_{5/2}, and the emitting state multiplet, ⁴G_{5/2}, can be expressed as (Eq. 3 and Eq. 4):⁴⁹

$$P_{i_{obs}}^{6H5/2} = \frac{I_{i \rightarrow j}^{rel}}{N \cdot B_{i \leftarrow j}^{rel}}, N = \sum_j \frac{I_{i \rightarrow j}^{rel}}{B_{i \leftarrow j}^{rel}} \quad \text{Eq. 3}$$

and

$$P_{j_{obs}}^{4G5/2} = \frac{I_{i \leftarrow j}^{rel}}{N \cdot A_{i \rightarrow j}^{rel}}, N = \sum_i \frac{I_{i \leftarrow j}^{rel}}{A_{i \rightarrow j}^{rel}} \quad \text{Eq. 4}$$

This observed thermal population is compared to the calculated Boltzmann distribution (Eq. 5):⁴⁹

$$P_{i_{calc}}^{system} = \frac{e^{-\frac{E_i}{k_B T}}}{\sum_i^{system} e^{-\frac{E_i}{k_B T}}} \quad \text{Eq. 5}$$

where is E_i is the energy of the i states in either the ground state multiplet, ⁶H_{5/2}, or emitting state multiplet, ⁴G_{5/2}. If each line in the emission and excitation spectra corresponds to a single electronic transition, the calculated and observed thermal population should be the same.⁴⁹ The observed population is evaluated by the use of a loss function. The model for the electronic energy levels described by the lowest loss value describes the system the best.

$$L = \sum_i 100 \cdot \frac{(P_{i_{obs}}^{6H5/2} - P_{i_{calc}}^{6H5/2})^2}{N} + \sum_i 100 \cdot \frac{(P_{i_{obs}}^{4G5/2} - P_{i_{calc}}^{4G5/2})^2}{N} \quad \text{Eq. 6}$$

This was used to resolve ambiguities in the interpretation of splitting of the energy levels determined from the spectra. Here the loss function is used to determine which of the different calculated populations agree with the observed population the best.

Results and discussion

To ensure reproducible results, all compounds were prepared in triplicates, and the unit cell determined for the crystals selected for investigation from each preparation, see the ESI for details.

Crystal Structure and Coordination Geometry

For all eight Eu³⁺ and Sm³⁺ compounds the single crystal structure was determined. Crystallographic information can be found in the ESI. Na₃[Eu(ODA)₃]·9H₂O crystallises in the monoclinic C2/c space group (CCDC deposition number 2291817) and was found to be isostructural to previously reported compound (CCDC entries DOFXIF 1143446 and DOFIX01 209363).^{61, 62} The Na₃[Sm(ODA)₃]·7H₂O compound crystallises in the monoclinic Cc space group. Na₃[Sm(ODA)₃]·7H₂O (CCDC deposition number 2291821) was found to be isostructural to the Na₃[Ln(ODA)₃]·7H₂O compounds, which has previously been reported for Eu³⁺ and Gd³⁺ (CCDC entries DOFXIF 1143446, DOFIX01 209363, and QUMYON 721017).⁶¹⁻⁶³ Figure 2a illustrates the donor atoms type and placement around the central Sm³⁺ ion. For both Na₃[Eu(ODA)₃]·8H₂O and Na₃[Sm(ODA)₃]·7H₂O three [ODA]²⁻ ligands coordinate to the central lanthanide(III) ion making it nine-coordinated. The complex is reported as having TTP coordination geometry.^{61, 62} The donor set is very symmetric and consists of nine oxygen atoms all originating from three [ODA]²⁻ molecules. Figure 2b shows the asymmetric unit, and Figure 2c illustrates the two Na₃[Sm(DPA)₃]·7H₂O complexes

placed within the unit cell. $\text{Na}_3[\text{Eu}(\text{ODA})_3]\cdot 9\text{H}_2\text{O}$ and $\text{Na}_3[\text{Sm}(\text{ODA})_3]\cdot 7\text{H}_2\text{O}$ differs by the space group, with a larger asymmetric unit for $\text{Na}_3[\text{Sm}(\text{ODA})_3]\cdot 7\text{H}_2\text{O}$ and less water molecules included in the structure. The crystallographic differences between the compounds are obvious, but let us consider the details.

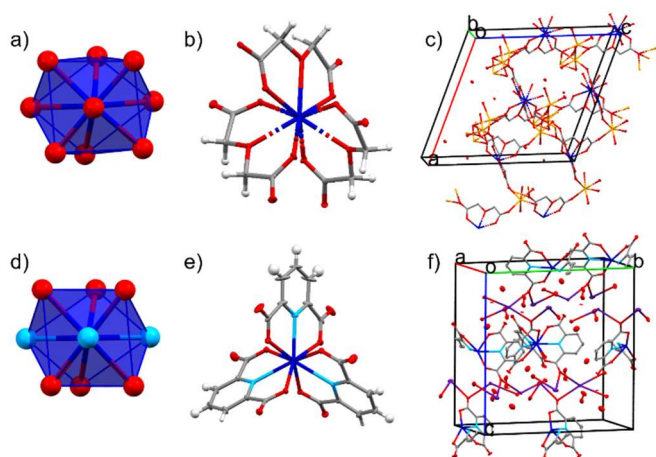


Figure 2. a) Polyhedra depicting coordination around the Sm^{3+} ion in $\text{Na}_3[\text{Sm}(\text{ODA})_3]\cdot 7\text{H}_2\text{O}$. b) molecular structure of $\text{Na}_3[\text{Sm}(\text{ODA})_3]\cdot 7\text{H}_2\text{O}$. c) The unit cell for the $\text{Na}_3[\text{Sm}(\text{ODA})_3]\cdot 7\text{H}_2\text{O}$ crystal structure. d) Polyhedra depicting coordination around the Sm^{3+} ion in $\text{Cs}_3[\text{Sm}(\text{DPA})_3]\cdot 9\text{H}_2\text{O}$. e) Molecular structure of $\text{Cs}_3[\text{Sm}(\text{DPA})_3]\cdot 9\text{H}_2\text{O}$. f) The unit cell for the $\text{Cs}_3[\text{Sm}(\text{DPA})_3]\cdot 9\text{H}_2\text{O}$ crystal structure. Colour code: Sm = dark blue, N = light blue, C = grey, O = red, and Cs = purple. Hydrogen atoms omitted for clarity. Thermal ellipsoids are at 50% probability.

The $\text{Cs}_3[\text{Eu}(\text{DPA})_3]\cdot 9\text{H}_2\text{O}$ crystallises in the orthorhombic $C222_1$ space group. The crystal created in the experimental section was found to twin, and the structure could not be determined. The Bravais lattice and unit cell agreed with the previously reported structure,⁵¹ and this crystal was used for single crystal luminescence measurements. However the structure analysis was done using the crystal structure by Brayshaw *et al.* (CCDC entry YOZRUA 1306070).⁵¹ The $\text{Cs}_3[\text{Sm}(\text{DPA})_3]\cdot 9\text{H}_2\text{O}$ crystallises in the orthorhombic $C222_1$ space group (CCDC deposition number 2291822). $\text{Cs}_3[\text{Sm}(\text{DPA})_3]\cdot 9\text{H}_2\text{O}$ was found to be isostructural to the $\text{Cs}_3[\text{Ln}(\text{DPA})_3]\cdot 9\text{H}_2\text{O}$ compounds, which has previously been reported for Ce^{3+} , Eu^{3+} , Tb^{3+} , and Yb^{3+} (CCDC entries FEMPUL, YOZRUA 1306070 1497223, HOYTEV 622323, and HOYTIZ 623104).^{50, 51, 64}

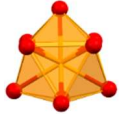

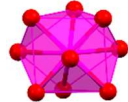
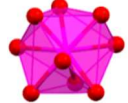
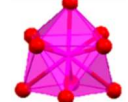
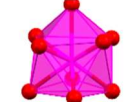
Figure 2d illustrates the donor atoms type and placement around the central Sm^{3+} ion. In $\text{Cs}_3[\text{Ln}(\text{DPA})_3]\cdot 9\text{H}_2\text{O}$ three $[\text{DPA}]^{2-}$ ligands coordinate to the central lanthanide(III) ion in a nine-coordinated TTP coordination geometry.^{34, 51, 65-68} The donor set consist of three nitrogen atoms placed in the tricapping layer, and six oxygen atoms in the two trigonal layers. All donor atoms originate from three coordinating $[\text{DPA}]^{2-}$ molecules. Figure 2e shows the asymmetric unit. Figure 2f illustrates the two $\text{Cs}_3[\text{Sm}(\text{DPA})_3]\cdot 9\text{H}_2\text{O}$ complexes placed within the unit cell. The four TTP systems differ by lanthanide— Eu^{3+} and Sm^{3+} —and the donor set: Two compounds with oxygen only and two compounds with three nitrogen six oxygen.

The $\text{Na}[\text{Eu}(\text{DOTA})\text{H}_2\text{O}]\cdot 4\text{H}_2\text{O}$ (CCDC deposition number 2291807) and $\text{Na}[\text{Sm}(\text{DOTA})\text{H}_2\text{O}]\cdot 4\text{H}_2\text{O}$ (CCDC deposition number 2291819) compounds were found to be isostructural. They crystallise in the trigonal $P-1$ space group as previously reported.^{69, 70} The compounds are reported to have the cSAP coordination geometry.^{69, 70 71 71} In the DOTA compounds, the donor set consists of four nitrogen atoms in the lower square

antiprism plane, and five oxygen atoms, with four originating from the $[\text{DOTA}]^{4-}$ in the upper square antiprism layer and a single water molecule in the capping position.

$\text{Na}[\text{Eu}(\text{EDTA})(\text{H}_2\text{O})_3]\cdot 5\text{H}_2\text{O}$ (CCDC deposition number 2291811) and $\text{Na}[\text{Sm}(\text{EDTA})(\text{H}_2\text{O})_3]\cdot 5\text{H}_2\text{O}$ (CCDC deposition number 2291820) were found to be isostructural and crystallises in the orthorhombic $Fdd2$ space group. They are isostructural to previously reported compounds.⁷²⁻⁷⁷ $\text{Na}[\text{Sm}(\text{EDTA})(\text{H}_2\text{O})_3]\cdot 5\text{H}_2\text{O}$ is described in literature as having cSAP coordination geometry.⁷⁸ The lanthanide(III) the donor set consist of two nitrogen atoms, with one occupying the capping position and the other being placed in the first square antiprism layer, and seven oxygen atoms, with four originating from $[\text{EDTA}]^{4-}$ and the other three from water molecules. As the structures of the eight compounds were determined, the site symmetry of the nine-coordinated Sm^{3+} polyhedra, could then be examined.

Table 1: σ_{ideal} values from AlignIt, for oxygen only coordination polyhedra for the Eu^{3+} compounds.

			
		cSAP (C_{4v})	TTP (D_{3h})
	$\text{Na}_3[\text{Eu}(\text{ODA})_3]\cdot 8\text{H}_2\text{O}$	1.26	0.76
	$\text{Cs}_3[\text{Eu}(\text{DPA})_3]\cdot 9\text{H}_2\text{O}$	1.87	0.89
	$\text{Na}[\text{Eu}(\text{DOTA})\text{H}_2\text{O}]\cdot 4\text{H}_2\text{O}$	0.38	1.48
	$\text{Na}[\text{Eu}(\text{EDTA})(\text{H}_2\text{O})_3]\cdot 5\text{H}_2\text{O}$	0.63	0.96

Evaluation of Coordination Geometry and Site Symmetry

The site symmetry of a lanthanide(III) complexes affects the crystal field splitting. Here a continuous symmetry measure was used to determine the coordination geometry and site symmetry. First, the deviation from ideal geometry is calculated. A continuous shape measure determines the distance between the real structure and ideal model polyhedra to find the most representative ideal structure, quantified by the symmetry deviation value, σ_{ideal} . The smallest σ_{ideal} value determines the ideal model that most closely resembles the real observed structure.^{2,3} This is achieved by the use of the AlignIt methodology.⁵⁵

Table 1 compares the relevant ideal polyhedra to create a comparative scale of different deviation values. Additional symmetry deviation values can be found in ESI. Nine-coordinated lanthanide(III) complexes are usually described as

having either a cSAP or a TTP coordination geometry.^{79, 80} Inspection of Table 1 shows that $\text{Na}_3[\text{Eu}(\text{ODA})_3]\cdot 8\text{H}_2\text{O}$ and $\text{Cs}_3[\text{Eu}(\text{DPA})_3]\cdot 9\text{H}_2\text{O}$ were found to have lowest σ_{ideal} values against the ideal TTP structure, in agreement with literature.^{34, 51, 65-68} The ODA complexes have the lower σ_{ideal} values, than the DPA complexes. As the Ln-N and Ln-O bond distances differs by 0.3 Å this is in good agreement with the more symmetric all oxygen donor set.^{68, 81} For the DOTA and EDTA complexes the lowest σ_{ideal} was observed against the ideal cSAP geometry, note that the EDTA donor set is asymmetric and will have no symmetry, but retains the shape of the model polyhedrons.^{71, 78} The σ_{ideal} deviation value made by AlignIt assumes an oxygen only donor set and uses uniform bond distances. As most lanthanide(III) compounds have a mixed donor set that vary in bond lengths, the σ_{ideal} -value does not describe the symmetry well, σ_{ideal} reports on geometry compared to a model geometry. To analyse the point group symmetry of the compounds, as point group symmetry deviation value or σ_{sym} was used. This method takes both coordination geometry and donor set into account.¹ Table 2 show the σ_{sym} -values calculated in the six relevant symmetries for both the donor set and the relevant molecular structure.

For the two compounds with TTP geometry. $\text{Na}_3[\text{Ln}(\text{ODA})_3]\cdot 8\text{H}_2\text{O}$ and $\text{Cs}_3[\text{Ln}(\text{DPA})_3]\cdot 9\text{H}_2\text{O}$, both the inner sphere coordination polyhedra are best described by D_3 symmetry. For D_{3h} a higher σ_{sym} -value was found, which indicate that none of the compounds contain a horizontal mirror plane. Interestingly, $\text{Cs}_3[\text{Ln}(\text{DPA})_3]\cdot 9\text{H}_2\text{O}$ has a perfect σ_{sym} value against D_3 , which may be caused by the biding angle of the ligands or the more rigid nature of the $[\text{DPA}]^{2-}$ ligand compared to $[\text{ODA}]^{2-}$. If we expand the evaluation to include the ligand backbone, we can see the $[\text{ODA}]^{2-}$ backbones are disordered, while the rigid $[\text{DPA}]^{2-}$ ligand also has high symmetry.

$\text{Na}[\text{Ln}(\text{DOTA})\text{H}_2\text{O}]\cdot 4\text{H}_2\text{O}$ was found to have high symmetry as the donor set is have C_{4v} point group symmetry, while the molecular structure perturbs the vertical mirror planes as these are not present in the $[\text{DOTA}]^{4-}$ ligand backbone. For coordination geometry of $\text{Na}[\text{Ln}(\text{EDTA})(\text{H}_2\text{O})_3]\cdot 5\text{H}_2\text{O}$ the σ_{sym} values are large, as the position of two nitrogen atoms results in only a single symmetry operation is present: a vertical mirror plane (C_v). If the EDTA ligand is included in the analysis $\text{Na}[\text{Ln}(\text{EDTA})(\text{H}_2\text{O})_3]\cdot 5\text{H}_2\text{O}$ has no symmetry. The symmetry analysis were done for both Sm^{3+} and Eu^{3+} compounds, see table 2. In the symmetric compounds, $\text{Na}_3[\text{Sm}(\text{ODA})_3]\cdot 8\text{H}_2\text{O}$ is slightly more disordered than $\text{Na}_3[\text{Eu}(\text{ODA})_3]\cdot 8\text{H}_2\text{O}$, while the molecular structure of the $[\text{EDTA}]^{4-}$ complexes are different not in all cases fully asymmetric. Following this analysis the $\text{Na}_3[\text{Ln}(\text{ODA})_3]\cdot 8\text{H}_2\text{O}$ and $\text{Cs}_3[\text{Ln}(\text{DPA})_3]\cdot 9\text{H}_2\text{O}$ compounds have TTP geometry with D_3 symmetry, $\text{Na}[\text{Ln}(\text{DOTA})\text{H}_2\text{O}]\cdot 4\text{H}_2\text{O}$ has cSAP geometry with C_4 symmetry, and $\text{Na}[\text{Ln}(\text{EDTA})(\text{H}_2\text{O})_3]\cdot 5\text{H}_2\text{O}$ has cSAP geometry with no (C_1) symmetry.

Table 2: Point group symmetry deviation values (σ_{sym})¹ for the real coordination polyhedra and the molecular structure for the Eu^{3+} compounds and the Sm^{3+} in parenthesis. Light pink indicates the point group with highest symmetry that describes the system.

Point group	$\text{Na}_3[\text{Eu}(\text{ODA})_3]\cdot 8\text{H}_2\text{O}$		$\text{Cs}_3[\text{Eu}(\text{DPA})_3]\cdot 9\text{H}_2\text{O}$		$\text{Na}[\text{Eu}(\text{DOTA})\text{H}_2\text{O}]\cdot 4\text{H}_2\text{O}$		$\text{Na}[\text{Eu}(\text{EDTA})(\text{H}_2\text{O})_3]\cdot 5\text{H}_2\text{O}$	
	Inner sphere	Molecular structure	Inner sphere	Molecular structure	Inner sphere	Molecular structure	Inner Sphere	Molecular structure
C_{4v}	3.2 (3.7)	23.5 (23.3)	25.1 (24.9)	30.7 (30.1)	0.8 (0.8)	5.8 (5.7)	31.1 (26.6)	36.0 (38.9)
C_4	2.6 (3.0)	27.2 (27.1)	30.9 (30.7)	35.7 (36.0)	0.1 (0.1)	0.5 (0.5)	32.9 (31.4)	32.9 (33.9)
D_{3h}	1.3 (1.6)	12.0 (12.5)	1.7 (1.8)	11.5 (11.1)	63.2 (63.1)	75.7 (77.6)	54.4 (54.1)	96.6 (91.6)
D_3	0.3 (0.4)	2.6 (3.2)	0.0 (0.0)	0.1 (0.1)	79.3 (79.2)	85.0 (85.0)	63.0 (62.5)	114.2 (109.8)
C_3	0.3 (0.5)	3.3 (3.9)	0.0 (0.0)	0.1 (0.1)	16.7 (16.7)	14.4 (14.4)	25.9 (26.0)	37.7 (39.3)
C_2	0.0 (0.2)	0 (1.0)	0.0 (0.0)	0.0 (0.0)	0.1 (0.1)	0.3 (0.3)	26.7 (23.5)	30.9 (41.0)

Table 3: The number of bands empirically observed in the $^5D_0 \rightarrow ^7F_J$ emission for different point group symmetries.²⁴ The table is a modified version of ref. ²⁷ The table also includes the number of observed bands in a different ODA compound with same coordination by Kirby et al.⁸²

$^5D_0 \rightarrow ^7F_J$	J = 0	J	J	J	J	J
		=	=	=	=	=
		1	2	3	4	5
C_{4v} and C_4	1	2	4	5	7	8
D_{3h}	1	2	3	5	6	7
C_{3v} and C_3	1	2	3	5	6	7
C_2	1	3	5	7	9	11
Kirby et al. ODA ⁸²	0	1	3	4	4	?

Luminescence Spectra

To examine the effect of the crystal field on the electronic structure of the central lanthanide ion emission and excitation spectra and luminescence lifetimes were recorded for single crystals at 298 K and microcrystalline powders at 77 K.

Eu³⁺ Compounds. For Eu³⁺ the number of lines is expected to be related to the point group symmetry of the compound,^{13, 24, 27, 31-33} as illustrated by the number of lines in each $^5D_0 \rightarrow ^7F_J$ multiplet in specific symmetries compiled in Table 3. Eu³⁺ compounds are useful model system for a crystal field analysis

as both the ground state (7F_0) and emitting state (5D_0) are non-degenerate,^{34, 35} but it must be recognised that the most of our analytical framework is empiric in nature,^{24, 27, 39} and with improved instrumentation we are now arriving at different results.^{26, 49} This is also the case here.

The two Eu compounds with cSAP geometry: Na[Eu(DOTA)H₂O]·4H₂O and Na[Eu(EDTA)(H₂O)₃]·5H₂O, were analysed first. In the luminescence spectre, shown in Figure 3, one line was observed for both the $^5D_0 \rightarrow ^7F_0$ band for both of the two cSAP species. This is predicted in Table 3 and also indicates that only one compound is present in the samples.²⁷ For the $^5D_0 \rightarrow ^7F_1$ band three lines were observed, which as expected for C_v, but higher splitting what is predicted for C_{4v}. We are investigating crystalline samples at 77K with modern equipment, which could explain why the empirical predictions fail.^{24, 27, 39} For the $^5D_0 \rightarrow ^7F_2$ band three lines were observed for Na[Eu(DOTA)H₂O]·4H₂O and Na[Eu(EDTA)(H₂O)₃]·5H₂O, which is a lower splitting than what is expected for both symmetries, showing that coincidental degeneracy also has a role to play. Due to low intensity, the $^5D_0 \rightarrow ^7F_3$ and $^5D_0 \rightarrow ^7F_5$ band is seldom resolved enough to include in an analysis. Here, the $^5D_0 \rightarrow ^7F_3$ band consist of two lines for both cSAP species, and only two lines are resolved in the $^5D_0 \rightarrow ^7F_5$ band for Na[Eu(DOTA)H₂O]·4H₂O and three lines for Na[Eu(EDTA)(H₂O)₃]·5H₂O. The resolution and total splitting of these multiplets makes it hard to differentiate between real and coincidental degeneracy. Finally, the $^5D_0 \rightarrow ^7F_4$ band has five

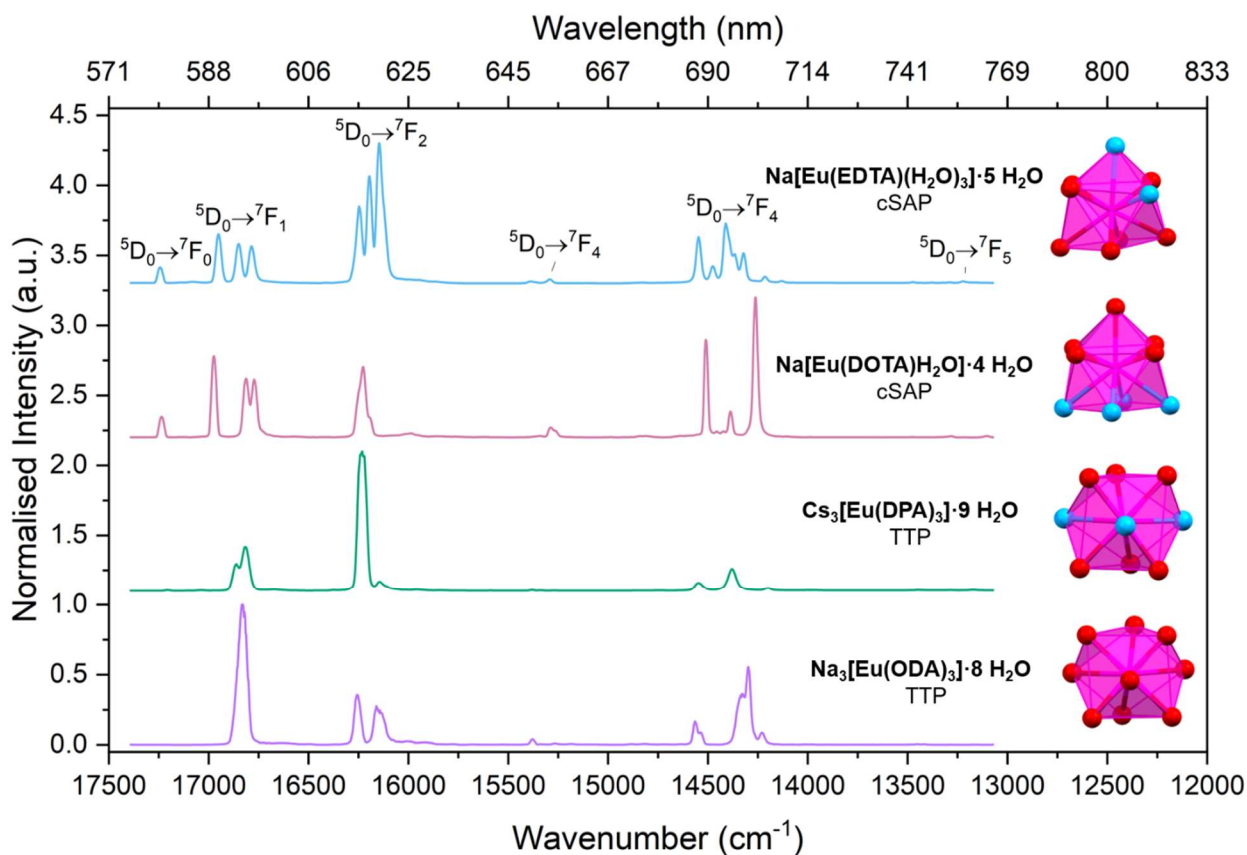


Figure 3. Normalised single crystal emission at (excitation at 394 nm) for Na₃[Eu(ODA)₃]·8H₂O, Cs₃[Eu(DPA)₃]·9H₂O, Na[Eu(DOTA)H₂O]·4H₂O and Na[Eu(EDTA)(H₂O)₃]·5H₂O at 77 K. Spectra normalised to the highest peak. Polyhedral depicts coordination around the Eu³⁺ ion.

observed lines in the $\text{Na}[\text{Eu}(\text{DOTA})\text{H}_2\text{O}]\cdot 4\text{H}_2\text{O}$ spectra compared and seven in the $\text{Na}[\text{Eu}(\text{EDTA})(\text{H}_2\text{O})_3]\cdot 5\text{H}_2\text{O}$ spectra. Also here the number of lines are lower than what is predicted for either symmetry. Although the resolution is better here, the total splitting larger, it is likely that the number of lines, can only be resolved at even lower temperatures.

Single crystals $\text{Na}[\text{Eu}(\text{DOTA})\text{H}_2\text{O}]\cdot 4\text{H}_2\text{O}$ has previously been analysed by Thomsen et al. and Parker et al.⁸³⁻⁸⁶ Our spectra are consistent with the their spectra. The failure of the empirical model given rise to the predictions in Table 3 has also been previously described.^{27, 29, 52, 83-87} We often find these descriptors only work for some multiplet in a spectrum, and that the symmetry reported by each multiplet in a spectrum can be different.

In the species with TTP geometry, $\text{Na}_3[\text{Eu}(\text{ODA})_3]\cdot 8\text{H}_2\text{O}$ has a ${}^5\text{D}_0 \rightarrow {}^7\text{F}_0$ line that cannot be observed, see Figure 3. This line is often barely detectable for the other compounds ascribed TTP geometry. The same is the case for $\text{Cs}_3[\text{Eu}(\text{DPA})_3]\cdot 9\text{H}_2\text{O}$ spectrum, see Figure 3. The lack of at ${}^5\text{D}_0 \rightarrow {}^7\text{F}_0$ band is often

explained not by the TTP geometry but by the D_{3h} symmetry. The line is only observed if there is not mirror plane perpendicular to the main rotational axis.²⁷ Even though the compounds was found to have D_3 symmetry, a σ_{sym} -values < 2 for the D_{3h} symmetry is low enough that the luminescence spectra have no ${}^5\text{D}_0 \rightarrow {}^7\text{F}_0$ line.

Continuing the analysis of the TTP compounds, we move to the ${}^5\text{D}_0 \rightarrow {}^7\text{F}_1$ band. Here, two lines were observed for $\text{Cs}_3[\text{Eu}(\text{DPA})_3]\cdot 9\text{H}_2\text{O}$ indicating a splitting of $m_j = \pm 1$ and $m_j = 0$. In contrast only one line was observed in the ${}^5\text{D}_0 \rightarrow {}^7\text{F}_1$ band of $\text{Na}_3[\text{Eu}(\text{ODA})_3]\cdot 8\text{H}_2\text{O}$. This indicates that all the electronic energy levels are degenerate, which is not predicted for any symmetries lower than cubic (not included in Table 3). The splitting of $m_j = \pm 1$ and $m_j = 0$ should occur in compounds with D_3/D_{3h} symmetry, but the splitting of these levels are not resolved in the data for $\text{Na}_3[\text{Eu}(\text{ODA})_3]\cdot 8\text{H}_2\text{O}$.^{9, 24, 27, 39, 82} An alternative explanation is that transitions from the $m_j = 0$ level is forbidden, we observe the splitting of $m_j = \pm 1$, but there is limited precedence for assuming that single m_j -states are pure

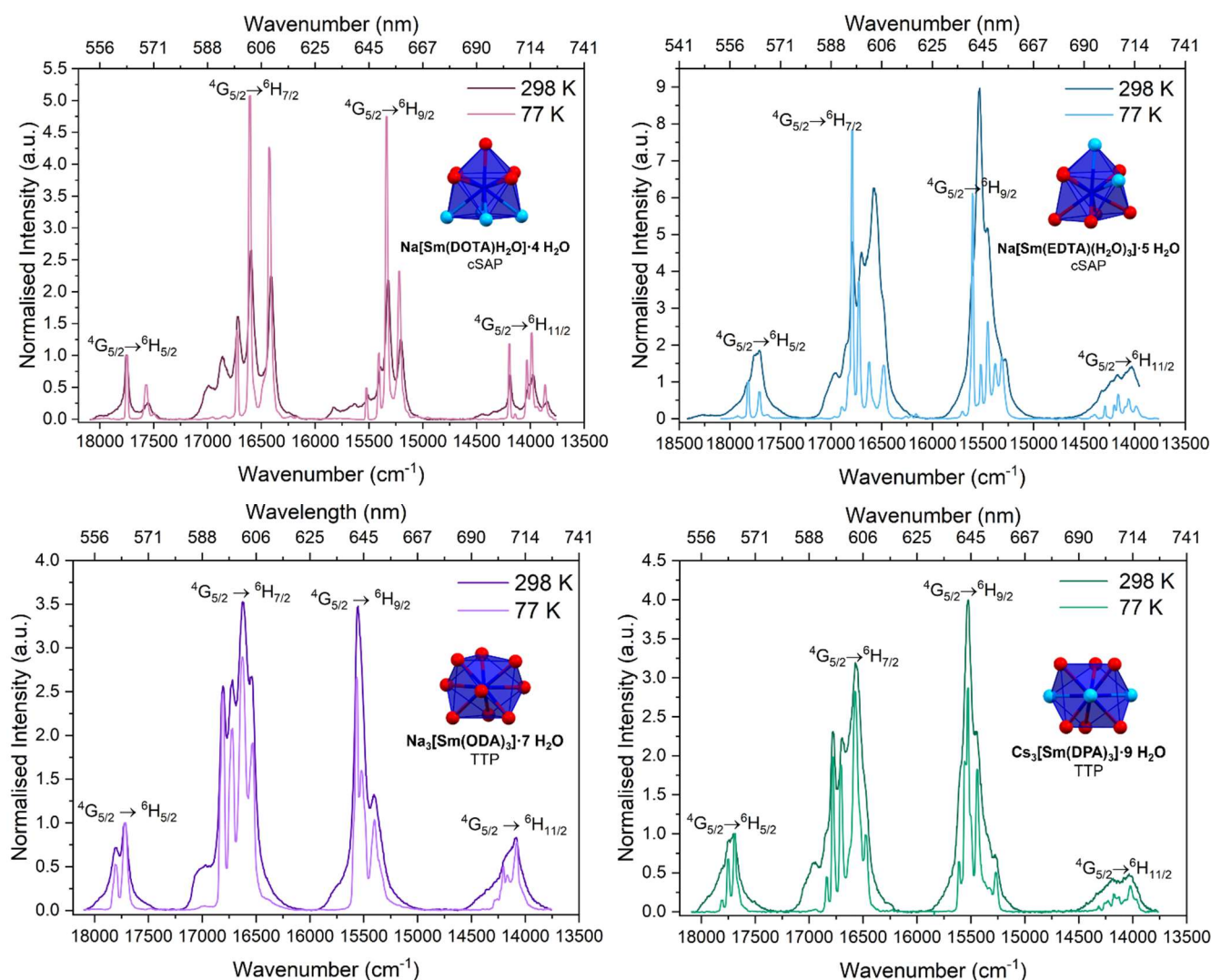


Figure 4: Normalised emission (excitation at 463 nm) for $\text{Na}_3[\text{Sm}(\text{ODA})_3]\cdot 7\text{H}_2\text{O}$, $\text{Cs}_3[\text{Sm}(\text{DPA})_3]\cdot 9\text{H}_2\text{O}$, $\text{Na}[\text{Sm}(\text{DOTA})\text{H}_2\text{O}]\cdot 4\text{H}_2\text{O}$ and $\text{Na}[\text{Sm}(\text{EDTA})(\text{H}_2\text{O})_3]\cdot 5\text{H}_2\text{O}$ at 77 K and 298 K. Normalised to the ${}^4\text{G}_{5/2} \rightarrow {}^6\text{H}_{5/2}$ band. Polyhedra depicts coordination around the Sm^{3+} ion.

states and retain a nature that changes the transition probabilities beyond the ${}^5D_0 \rightarrow {}^7F_0$ line.^{9, 24, 27, 39} In D_3/D_{3h} symmetry the 7F_1 and 7F_2 m_J -states could be pure states, and with $m_J = 0$ forbidden, only degenerate bands for $m_J = \pm 1$ and $m_J = 2$ would be observed. However, the 7F_3 , 7F_4 , and 7F_5 bands does not contain a pure $m_J = 0$ state as it must mix with the $m_J = \pm 3$ states. In D_3 symmetry (TTP structures) the following crystal field parameters are needed: B_0^2 , B_0^4 , B_0^6 , B_3^4 , B_3^6 , and B_6^6 . The off-diagonal terms results in m_J mixing when $\Delta m_J \geq 3$.^{8, 70, 86, 88}

For $Cs_3[Eu(DPA)_3] \cdot 9H_2O$ two and three lines were observed for the ${}^5D_0 \rightarrow {}^7F_2$ and ${}^5D_0 \rightarrow {}^7F_4$ band, respectively. This indicates a larger splitting than what is predicted in Table 3 for D_3 point group symmetry.^{9, 24, 27, 39} Even though the two compounds, $Na_3[Eu(ODA)_3] \cdot 8H_2O$ and $Cs_3[Eu(DPA)_3] \cdot 9H_2O$, are both best described by TTP geometry and both have D_3 symmetry, the observed splitting in the emission spectra are different.

Overall, the Eu^{3+} model compounds does not follow the empirical predictions shown in Table 3, and beyond the influence of horizontal mirror planes, we are left to determine the electronic structure of the Sm^{3+} compounds before we can compare the properties of the two ions.

Sm^{3+} Compounds. In Sm^{3+} ion the simplest transition from the emitting multiplet to the lowest multiplet, ${}^4G_{5/2} \rightarrow {}^6H_{5/2}$ is a multiplet with nine lines.⁴¹ This correspond to the first band in the spectra shown in Figure 4. For the two Sm^{3+} compounds with cSAP geometry, $Na[Sm(DOTA)H_2O] \cdot 5H_2O$ and $Na[Sm(EDTA)(H_2O)_3] \cdot 5H_2O$, fewer lines were observed in all bands in the emission spectra at 77K compared to the two compounds with TTP geometry.

For $Na[Sm(DOTA)H_2O] \cdot 4H_2O$ three lines were observed for the ${}^4G_{5/2} \rightarrow {}^6H_{5/2}$ band, indicating a maximum splitting of ${}^6H_{5/2}$ and only one of the m_J levels in ${}^4G_{5/2}$ with a significant population at 77 K, thus indicating a large crystal field splitting, resulting in the lines origin from transition from higher m_J levels in ${}^4G_{5/2}$ having too small intensity to be observed. In support of this hypothesis, four, five, and six lines were observed for the For the ${}^4G_{5/2} \rightarrow {}^6H_{7/2}$, ${}^4G_{5/2} \rightarrow {}^6H_{9/2}$, and ${}^4G_{5/2} \rightarrow {}^6H_{11/2}$ bands, respectively. This number of lines corresponds to the maximum splitting for ${}^6H_{5/2}$, ${}^6H_{7/2}$, ${}^6H_{9/2}$, and ${}^6H_{11/2}$, respectively.

For $Na[Sm(EDTA)(H_2O)_3] \cdot 5H_2O$ four lines were observed for the ${}^4G_{5/2} \rightarrow {}^6H_{5/2}$ band. Also, for the ${}^4G_{5/2} \rightarrow {}^6H_{7/2}$, ${}^4G_{5/2} \rightarrow {}^6H_{9/2}$, and ${}^4G_{5/2} \rightarrow {}^6H_{11/2}$ bands more lines were observed than the maximum splitting in ${}^6H_{5/2}$, ${}^6H_{7/2}$, ${}^6H_{9/2}$, and ${}^6H_{11/2}$, respectively. This indicates that two m_J levels in ${}^4G_{5/2}$ are populated at 77K, but the splitting for the ground state multiplet, ${}^6H_{5/2}$, and the first emitting multiplet, ${}^4G_{5/2}$, might be quite similar, as this would explain why six lines are not observed, but instead four, for the ${}^4G_{5/2} \rightarrow {}^6H_{5/2}$ band. With similar splitting, some of the lines will overlap, and four lines can be observed.

For the two Sm^{3+} compounds with TTP geometry, $Na_3[Sm(ODA)_3] \cdot 7H_2O$ and $Cs_3[Sm(DPA)_3] \cdot 9H_2O$, a similar spectral shape was observed in the emission spectra, see Figure 4. The ${}^4G_{5/2} \rightarrow {}^6H_{5/2}$ band shows three lines at 77K. The emission spectra reflects the population of the three m_J levels in ${}^4G_{5/2}$, and for transitions to be observed with visible intensity, this requires significant population of each m_J levels. As the transition end in the ${}^6H_{5/2}$ multiplet, transitions to all of these

states are expected to be observed independent of the temperature.⁴⁹ For three lines to be observed for the ${}^4G_{5/2} \rightarrow {}^6H_{5/2}$ band this either indicates that only one state in the first emitting multiplet ${}^4G_{5/2}$ is populated or the ground multiplet ${}^6H_{5/2}$ does not have the maximum splitting. If ${}^6H_{5/2}$ does not have the maximum splitting, this would indicate a more symmetric nature of two compounds with TTP geometry and D_3/D_{3h} symmetry than what was observed for the compound with cSAP coordination geometry and C_4 symmetry (Table 2). This is in agreement with the observations done off for the Eu^{3+} model compounds. Note that $Na[Sm(EDTA)(H_2O)_3] \cdot 5H_2O$ compound has cSAP coordination geometry, but not symmetry and will not be considered in symmetry arguments.

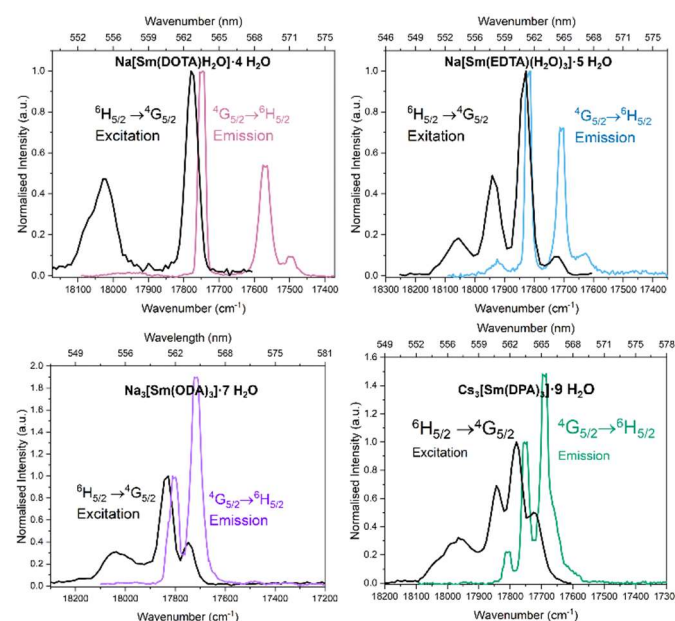


Figure 5: Normalised emission (excitation at 463 nm) recorded at 77 K normalised to the ${}^4G_{5/2} \rightarrow {}^6H_{5/2}$ band. Normalised powdered excitation (emission scan from 520 nm to 580 nm) recorded at 77 K normalised to the ${}^4G_{5/2} \leftarrow {}^6H_{5/2}$ band. The spectra were normalised to the transition from the lowest m_J state in the ground state multiplet (${}^6H_{5/2}$) to the lowest m_J state in the first emitting state multiplet (${}^4G_{5/2}$).

For the ${}^4G_{5/2} \rightarrow {}^6H_{7/2}$ and ${}^4G_{5/2} \rightarrow {}^6H_{9/2}$ bands more lines than the maximum splitting for ${}^6H_{7/2}$ and ${}^6H_{9/2}$ (4 and 5 m_J levels, respectively) is seen. This indicates that two of the states in ${}^4G_{5/2}$ is thermally populated to a degree where we easily observe transitions from the levels. This is also confirmed by the fact that the amount of lines observed for each band in the emission spectra does not increase threefold at 298 K, see Figure 4.^{37, 41, 48} The spectra at 298 K show how the thermal population of the states changes as well as thermal broadening of the peaks. Additionally, at 298 K the bands appear significantly broader compared to at 77 K, indicating additional lines appearing from a change in the population within the excited state multiplet population, see Figure 4. At 298 K all three states in emitting ${}^4G_{5/2}$ multiplet are populated at 298K. Considering the two Sm^{3+} compounds with TTP geometry, $Na_3[Sm(ODA)_3] \cdot 7H_2O$ and $Cs_3[Sm(DPA)_3] \cdot 9H_2O$, these display the same spectral features, suggesting a very small splitting of two of the electronic energy levels in the ${}^6H_{5/2}$ multiplet. For a Kramer's ion such as Sm^{3+} the maximum splitting of three would be expected.^{9, 37, 46-48} When investigating the electronic energy levels through a Boltzmann distribution, we found that the

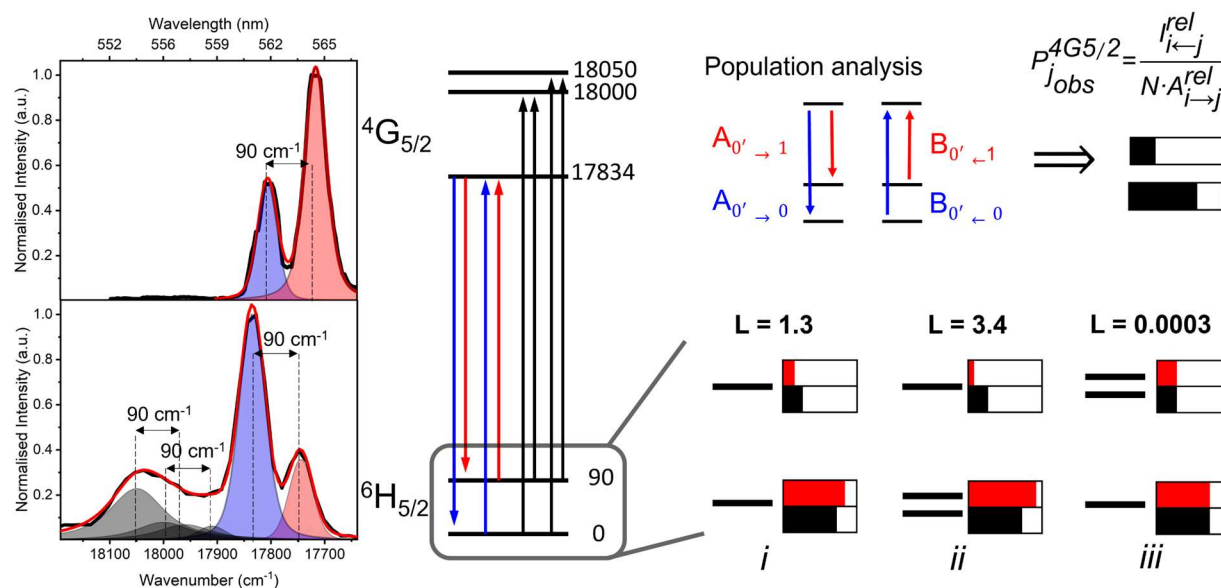


Figure 6. Top left: Normalised powdered emission (excitation at 463 nm) recorded of $\text{Na}_3[\text{Sm}(\text{ODA})_3] \cdot 7\text{H}_2\text{O}$ at 77 K normalised to the most intense line in ${}^4\text{G}_{5/2} \rightarrow {}^6\text{H}_{5/2}$ band. The spectra has been fitted with two Voigt functions where the splitting between the two lines are the splitting of the levels in ${}^6\text{H}_{5/2}$. Bottom left: Normalised powdered excitation (emission scan from 520 nm to 580 nm) recorded of $\text{Na}_3[\text{Sm}(\text{ODA})_3] \cdot 7\text{H}_2\text{O}$ at 77 K where the spectra has been fitted with Voigt functions with shared parameters. Right top: From the spectral intensities an observed population (P) is determined from the relative intensities (I) and the relative transition probability (A,B). Bottom right: Evaluation of three different models for the electronic structure of the ${}^6\text{H}_{5/2}$ multiplet (1), (2), and (3). The black and red bars shows the calculated Boltzmann population at 77 K (the red bar) and 298 K (the black bar) are shown along the calculated Loss number (L) for each model is shown.

splitting of both ${}^6\text{H}_{5/2}$ and ${}^4\text{G}_{5/2}$ multiplets is of a magnitude where two of the three states (in both ${}^6\text{H}_{5/2}$ and ${}^4\text{G}_{5/2}$) be observed. This assumption is confirmed by the excitation spectra and supported in the other transitions in the emission spectra. That only three and not six lines are observed for the the ${}^4\text{G}_{5/2} \rightarrow {}^6\text{H}_{5/2}$ band could either be a result of this band being weaker in intensity compared to some of the other emission bands, which lead us to investigate further.

Deconvoluting the Electronic Energy Levels for Sm^{3+}

Compared to Eu^{3+} , the crystal field splitting in Sm^{3+} compounds cannot be “directly” estimated from number of peaks and the energy splitting between them in the spectra.^{8, 9, 37, 41-44, 46, 48, 89-92} Instead, this requires the understanding of precisely which electronic energy levels the transition happens from and to, and what line each transition corresponds to. This requires good spectral resolution, and the analysis can be made simpler by having the spectra at different temperatures, where the population of the electronic energy levels change. Here, we record the spectra at 77 K and 298 K, see Figure 4. The lines in the ${}^4\text{G}_{5/2} \rightarrow {}^6\text{H}_{5/2}$ band are recovered from emission spectra and the lines in the ${}^4\text{G}_{5/2} \leftarrow {}^6\text{H}_{5/2}$ band are recovered from the excitation, see Figure 5. Each band were fitted to a sum of Voigt functions (see ESI for details), where each non-degenerate line is described by a single Voigt function. In the fit, the Gaussian width applied for is the instrumental broadening plus structural fluctuations, and the Lorentzian broadening is associated with the electronic transition. Fixing the Gaussian width was assumed to be a valid assumption for these samples.⁴⁹ Using these fit in our Boltzmann population analysis, the electronic energy levels in the four Sm^{3+} compounds were obtained. The best solution was found using a Loss function.

This method relies on the intensities being representative of the transition probability, which could be an issue in the case of different emitting species. As the powders were monophasic, and as only one species was seen in the Eu^{3+} compounds, we assume that only one emitting species is present in the samples. Further, in the case of $\text{Na}_3[\text{Sm}(\text{ODA})_3] \cdot 7\text{H}_2\text{O}$, the spectra were identical when measured on a single crystal and a single crystal crushed to a powder, see ESI.

Figure 6 shows how the electronic energy levels for $\text{Na}_3[\text{Sm}(\text{ODA})_3] \cdot 7\text{H}_2\text{O}$ were determined. Briefly, we start by investigating the two lines observed in the emission spectrum. Here we assume that only one of the three levels in ${}^4\text{G}_{5/2}$ are significantly populated for transitions to have an observable intensity. The observed lines are then to all the levels in ${}^6\text{H}_{5/2}$. Since only two lines are observed, three different electronic structures of the ${}^6\text{H}_{5/2}$ multiplet are possible: *i*) only two energy levels exist ${}^6\text{H}_{5/2}$ (0,1). *ii*) The two lowest energy levels in ${}^6\text{H}_{5/2}$ are degenerate ${}^6\text{H}_{5/2}$ (0,0,1). And *iii*) The two highest energy levels in ${}^6\text{H}_{5/2}$ are degenerate ${}^6\text{H}_{5/2}$ (0,1,1).

To select the correct electronic structure we used our Boltzmann population analysis, see Figure 6. This analysis computes state populations, compare models using a Loss function, and clearly show the model *iii*) is the correct electronic structure for $\text{Na}_3[\text{Sm}(\text{ODA})_3] \cdot 7\text{H}_2\text{O}$. The analysis for the other three compounds can be found in the ESI. The resulting electronic energy levels are shown in Figure 7. The determined crystal field splitting for Sm^{3+} in the four compounds, confirms the initial qualitative assignments done based on the spectra alone, but we now have a figure of merit, and can trust the assignments.

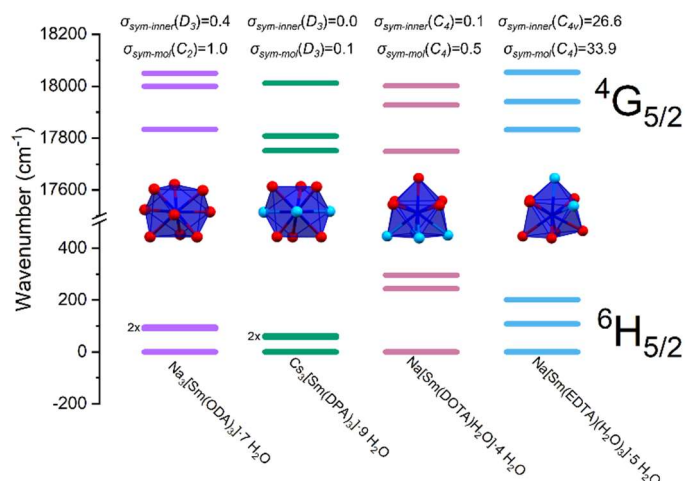


Figure 7: Dieke diagram for the energy levels from the ground state multiplet (${}^6H_{5/2}$) and first emitting state multiplet (${}^4G_{5/2}$) for the Sm^{3+} compounds resolved at 77 K. Symmetry deviation values (σ_{sym})³³ are shown above. $\sigma_{sym-inner}$ indicate the symmetry deviation value for the inner sphere coordination polyhedral and $\sigma_{sym-mol}$ indicate the symmetry deviation value for the molecular structure.

Figure 7 shows that a larger total splitting occur in the two compounds with cSAP geometry, $Na[Sm(DOTA)H_2O] \cdot 4H_2O$ and $Na[Sm(EDTA)(H_2O)_3] \cdot 5H_2O$, compared to the two compounds with TTP geometry and D_3/D_{3h} symmetry, $Na_3[Sm(ODA)_3] \cdot 7H_2O$ and $Cs_3[Sm(DPA)_3] \cdot 9H_2O$. The splitting pattern of ${}^6H_{5/2}$ $Na_3[Sm(ODA)_3] \cdot 7H_2O$ and $Cs_3[Sm(DPA)_3] \cdot 9H_2O$ are similar, but in ${}^4G_{5/2}$ it is reversed. We cannot say why, yet, but we can conclude that over-all, the crystal field splitting of the multiplets follow symmetry and lower values of ${}^6H_{5/2}$ multiplet splitting and less degenerate lines are observed in the compounds with a the D_3/D_{3h} symmetry compared those without mirror planes perpendicular to the main rotational axis. The splitting of the ${}^4G_{5/2}$ is of similar magnitude for all—high and low—symmetries, but a grouping of the states occur when symmetry is introduced.

Conclusions

In this study four Sm^{3+} compounds were made and compared to four isostructural Eu^{3+} model compounds. Two new compounds were reported: $Na_3[Sm(ODA)_3] \cdot 7H_2O$ and $Cs_3[Sm(DPA)_3] \cdot 9H_2O$. They were both found to have TTP coordination geometry, quantified with the AlignIt method, and they were shown to have D_3 symmetry by calculating the σ_{sym} -values. The shape and symmetry was evaluated for all eight coordination compounds. To evaluate the electronics structure, the luminescent properties of the compounds were characterised at 77 K and 298 K. By using a Boltzmann population analysis, the electronic energy levels in the Sm^{3+} compounds were determined. Generally, a larger splitting was observed for the two lower symmetry compounds, $Na[Sm(DOTA)H_2O] \cdot 4H_2O$ and $Na[Sm(EDTA)(H_2O)_3] \cdot 5H_2O$, compared to the two higher symmetry compounds, $Na_3[Sm(ODA)_3] \cdot 7H_2O$ and $Cs_3[Sm(DPA)_3] \cdot 9H_2O$. This takes the first steps towards understanding the crystal field splitting in Sm^{3+} compounds.

Conflicts of interest

There are no conflicts to declare.

Acknowledgements

We thank the Villum Foundation, the Carlsberg Foundation, and the University of Copenhagen for financial support.

Notes and references

- V. R. M. Nielsen, B. Le Guennic and T. J. Sørensen, *chemrxiv*, 2024, DOI: 10.26434/chemrxiv-2024-qr84c.
- V. Balaram, *Geoscience Frontiers*, 2019, **10**, 1285-1303.
- S. Cotton, *Lanthanide and actinide chemistry*, John Wiley & Sons, 2013.
- J.-C. G. Bünzli and S. V. Eliseeva, *Chemical Science*, 2013, **4**, 1939-1949.
- W. Carnall, P. Fields and K. Rajnak, *The Journal of chemical physics*, 1968, **49**, 4424-4442.
- W. T. Carnall, P. Fields and B. Wybourne, *The Journal of Chemical Physics*, 1965, **42**, 3797-3806.
- F. A. Cotton, G. Wilkinson and P. L. Gaus, *Basic inorganic chemistry*, John Wiley & Sons, 1995.
- A. de Bettencourt-Dias, *Luminescence of lanthanide ions in coordination compounds and nanomaterials*, John Wiley & Sons, 2014.
- S. V. Eliseeva and J.-C. G. Bünzli, *Chemical Society Reviews*, 2010, **39**, 189-227.
- C. N. Dansholm, A. K. R. Junker, L. G. Nielsen, N. Kofod, R. Pal and T. J. Sørensen, *ChemPlusChem*, 2019, **84**, 1778-1788.
- I. Hemmilä, S. Dakubu, V.-M. Mikkala, H. Siitari and T. Lövgren, *Analytical biochemistry*, 1984, **137**, 335-343.
- G. Vereb, E. Jares-Erijman, P. R. Selvin and T. M. Jovin, *Biophysical journal*, 1998, **74**, 2210-2222.
- W. D. Horrocks Jr and D. R. Sudnick, *Accounts of Chemical Research*, 1981, **14**, 384-392.
- X. Zhu, X. Wang, H. Zhang and F. Zhang, *Angewandte Chemie*, 2022, **134**, e202209378.
- M. Wang, C. Hu and Q. Su, *Biosensors*, 2022, **12**, 131.
- R. Arppe and T. J. Sørensen, *Nature Reviews Chemistry*, 2017, **1**, 1-13.
- S. J. Butler, M. Delbianco, L. Lamarque, B. K. McMahon, E. R. Neil, R. Pal, D. Parker, J. W. Walton and J. M. Zwieter, *Dalton Transactions*, 2015, **44**, 4791-4803.
- S. J. Butler, L. Lamarque, R. Pal and D. Parker, *Chemical Science*, 2014, **5**, 1750-1756.
- P. Caravan, J. J. Ellison, T. J. McMurphy and R. B. Lauffer, *Chemical reviews*, 1999, **99**, 2293-2352.
- J. Luzon and R. Sessoli, *Dalton Transactions*, 2012, **41**, 13556-13567.
- P. Zhang, L. Zhang, C. Wang, S. Xue, S.-Y. Lin and J. Tang, *Journal of the American Chemical Society*, 2014, **136**, 4484-4487.
- D. Parker, *Coordination Chemistry Reviews*, 2000, **205**, 109-130.
- G. H. Dieke, 1968.
- K. Binnemans, *Coordination Chemistry Reviews*, 2015, **295**, 1-45.
- J. M. Clemente-Juan, E. Coronado and A. Gaita-Ariño, *Lanthanides and Actinides in Molecular Magnetism*, 2015, **12**, 27-59.
- P. R. Nawrocki and T. J. Sørensen, *Physical Chemistry Chemical Physics*, 2023, **25**, 19300-19336.
- P. A. Tanner, *Chemical Society Reviews*, 2013, **42**, 5090-5101.

28. T. Cheisson and E. J. Schelter, *Science*, 2019, **363**, 489-493.
29. D. Parker, in *Handbook on the Physics and Chemistry of Rare Earths*, Elsevier, 2016, vol. 50, pp. 269-299.
30. B. G. Wybourne, *Journal of alloys and compounds*, 2004, **380**, 96-100.
31. J. C. G. Bünzli and G. O. Pradervand, *The Journal of Chemical Physics*, 1986, **85**, 2489-2497.
32. W. D. Horrocks Jr and D. R. Sudnick, *Science*, 1979, **206**, 1194-1196.
33. G. B. Jean-claude, *Inorganica Chimica Acta*, 1987, **139**, 219-222.
34. P. R. Nawrocki, N. Kofod, M. Juelsholt, K. M. Jensen and T. J. Sørensen, *Physical Chemistry Chemical Physics*, 2020, **22**, 12794-12805.
35. N. Kofod, P. Nawrocki, M. Juelsholt, T. L. Christiansen, K. M. Jensen and T. J. Sørensen, *Inorganic chemistry*, 2020, **59**, 10409-10421.
36. C. Görller-Walrand and K. Binnemans, *Handbook on the physics and chemistry of rare earths*, 1996, **23**, 121-283.
37. X. Chen, M. Jensen and G. Liu, *The Journal of Physical Chemistry B*, 2005, **109**, 13991-13999.
38. S. S. Mortensen, M. A. M. Nielsen, P. R. Nawrocki and T. J. Sørensen, 2022.
39. K. Binnemans and C. Görller-Walrand, *Chemical physics letters*, 1995, **245**, 75-78.
40. W. Carnall, P. Fields and K. Rajnak, *The Journal of Chemical Physics*, 1968, **49**, 4450-4455.
41. S. S. Mortensen, M. A. Marciniak Nielsen, P. Nawrocki and T. J. Sørensen, *The Journal of Physical Chemistry A*, 2022, **126**, 8596-8605.
42. B.-L. An, M.-L. Gong, M.-X. Li and J.-M. Zhang, *Journal of Molecular Structure*, 2004, **687**, 1-6.
43. S. Mohan, S. Kaur, D. Singh and P. Kaur, *Optical Materials*, 2017, **73**, 223-233.
44. O. Chukova, S. Nedilko, Z. Moroz and M. Pashkovskiy, *Journal of luminescence*, 2003, **102**, 498-503.
45. I. Kebaïli and M. Dammak, *Journal of Luminescence*, 2012, **132**, 2092-2097.
46. A. Lupei, C. Tiseanu, C. Gheorghe and F. Voicu, *Applied Physics B*, 2012, **108**, 909-918.
47. R. Skaudzius, S. Sakirzanovas and A. Kareiva, *Journal of Electronic Materials*, 2018, **47**, 3951-3956.
48. S. Sakirzanovas, A. Katelnikovas, H. Bettentrup, A. Kareiva and T. Jüstel, *Journal of Luminescence*, 2011, **131**, 1525-1529.
49. V. R. M. Nielsen, P. R. Nawrocki and T. J. Sørensen, *The Journal of Physical Chemistry A*, 2023, DOI: 10.1021/acs.jpca.3c00233.
50. G. Kervern, A. d'Aléo, L. Toupet, O. Maury, L. Emsley and G. Pintacuda, *Angewandte Chemie International Edition*, 2009, **48**, 3082-3086.
51. P. A. Brayshaw, J.-C. G. Buenzli, P. Froidevaux, J. M. Harrowfield, Y. Kim and A. N. Sobolev, *Inorganic Chemistry*, 1995, **34**, 2068-2076.
52. M. S. Thomsen, A. S. Anker, L. Kacenauskaite and T. J. Sørensen, *Dalton Transactions*, 2022, **51**, 8960-8963.
53. O. V. Dolomanov, L. J. Bourhis, R. J. Gildea, J. A. Howard and H. Puschmann, *Journal of applied crystallography*, 2009, **42**, 339-341.
54. G. M. Sheldrick, *Acta Crystallographica Section C: Structural Chemistry*, 2015, **71**, 3-8.
55. M. S. Thomsen, A. S. Anker, L. Kacenauskaite and T. J. Sørensen, 2022.
56. C. F. Macrae, I. Sovago, S. J. Cottrell, P. T. Galek, P. McCabe, E. Pidcock, M. Platings, G. P. Shields, J. S. Stevens and M. Towler, *Journal of applied crystallography*, 2020, **53**, 226-235.
57. S. S. Mortensen and T. J. Sørensen, *European Journal of Inorganic Chemistry*, 2023, e202300159.
58. P. R. Nawrocki, V. R. Nielsen and T. J. Sørensen, *Methods and Applications in Fluorescence*, 2022, **10**, 045007.
59. L. A. Deschenes and A. David A. Vanden Bout University of Texas, *Journal*, 2000.
60. *Journal*, 2018.
61. M. Albin, R. R. Whittle and W. D. Horrocks Jr, *Inorganic Chemistry*, 1985, **24**, 4591-4594.
62. F. A. Cotton and P. Huang, *Inorganica chimica acta*, 2003, **346**, 223-226.
63. A. Lennartson and M. Håkansson, *CrystEngComm*, 2009, **11**, 1979-1986.
64. S. M. Elahi and M. V. Rajasekharan, *ChemistrySelect*, 2016, **1**, 6515-6522.
65. D. Zhou, C. Huang, K. Wang and G. Xu, *Polyhedron*, 1994, **13**, 987-991.
66. J.-G. Kim, S.-K. Yoon, Y. Sohn and J.-G. Kang, *Journal of alloys and compounds*, 1998, **274**, 1-9.
67. M. Autillo, M. A. Islam, J. Jung, J. Pilmé, N. Galland, L. Guerin, P. Moisy, C. Berthon, C. Tamain and H. Bolvin, *Physical Chemistry Chemical Physics*, 2020, **22**, 14293-14308.
68. J. Salaam, I. N'Dala-Louika, C. Balogh, I. Suleimanov, G. Pilet, L. Veyre, C. Camp, C. Thieuleux, F. Riobé and O. Maury, *European Journal of Inorganic Chemistry*, 2022, **2022**, e202200412.
69. F. Benetollo, G. Bombieri, S. Aime and M. Botta, *Acta Crystallographica Section C: Crystal Structure Communications*, 1999, **55**, 353-356.
70. M. Briganti, E. Lucaccini, L. Chelazzi, S. Ciattini, L. Sorace, R. Sessoli, F. Totti and M. Perfetti, *Journal of the American Chemical Society*, 2021, **143**, 8108-8115.
71. S. Aime, A. Barge, F. Benetollo, G. Bombieri, M. Botta and F. Uggeri, *Inorganic Chemistry*, 1997, **36**, 4287-4289.
72. T. F. Koetzle, *Acta Crystallographica Section A: Cryst. Phys., Diffr., Theor. Crystallography.*, 1975, **31**.
73. L. Templeton, D. Templeton, A. Zalkin and H. Ruben, *Acta Crystallographica Section B: Structural Crystallography and Crystal Chemistry*, 1982, **38**, 2155-2159.
74. D. W. Engel, F. Takusagawa and T. F. Koetzle, *Acta Crystallographica Section C: Crystal Structure Communications*, 1984, **40**, 1687-1693.
75. J. Wang, P. Hu, B. Liu, L. Q. Zhang, G. X. Han, R. Xu and X. D. Zhang, *Zhurnal Neorganisheskoi Khimii*, 2010, **55**.
76. K. Nakamura, T. Kurisaki, H. Wakita and T. Yamaguchi, *Acta Crystallographica Section C: Crystal Structure Communications*, 1995, **51**, 1559-1563.
77. R. J. Holmberg, I. Korobkov and M. Murugesu, *RSC advances*, 2016, **6**, 72510-72518.
78. R. Ragul and B. Sivasankar, *Synthesis and Reactivity in Inorganic, Metal-Organic, and Nano-Metal Chemistry*, 2013, **43**, 382-389.
79. J. J. Thomson, *The London, Edinburgh, and Dublin Philosophical Magazine and Journal of Science*, 1904, **7**, 237-265.

80. M. G. Drew, *Coordination Chemistry Reviews*, 1977, **24**, 179-275.
81. P. A. Brayshaw, A. K. Hall, W. T. Harrison, J. M. Harrowfield, D. Pearce, T. M. Shand, B. W. Skelton, C. R. Whitaker and A. H. White, *Journal*, 2005.
82. A. F. Kirby and F. S. Richardson, *The Journal of Physical Chemistry*, 1983, **87**, 2557-2563.
83. M. S. Thomsen, H. O. B. Andersen and T. J. Sørensen, *Dalton Transactions*, 2022, **51**, 14118-14124.
84. M. S. Thomsen, A. O. Madsen and T. J. Sørensen, *Acta Crystallographica Section C*, 2021, **77**, 354-364.
85. M. Woods, S. Aime, M. Botta, J. A. K. Howard, J. M. Moloney, M. Navet, D. Parker, M. Port and O. Rousseaux, *Journal of the American Chemical Society*, 2000, **122**, 9781-9792.
86. D. Parker, E. A. Suturina, I. Kuprov and N. F. Chilton, *Accounts of Chemical Research*, 2020, **53**, 1520-1534.
87. R. S. Dickins, D. Parker, J. I. Bruce and D. J. Tozer, *Dalton Transactions*, 2003, 1264-1271.
88. J. D. Rinehart and J. R. Long, *Chemical Science*, 2011, **2**, 2078-2085.
89. W. Carnall, G. Goodman, K. Rajnak and R. Rana, *The Journal of chemical physics*, 1989, **90**, 3443-3457.
90. G. H. Dieke, *Spectra and Energy Levels of Rare Earth Ions in Crystals*, 1968.
91. S. K. Gupta, P. S. Ghosh, N. Pathak, A. Arya and V. Natarajan, *RSC Adv.*, 2014, **4**, 29202-29215.
92. S. K. Gupta, N. Pathak, S. K. Thulasidas and V. Natarajan, *Journal of Luminescence*, 2016, **169**, 669-673.
93. V. R. M. Nielsen, Sørensen, Thomas J., 2024.